Journal of Vacuum Science and Technology A, 23, (2005) 1055-1060

Epitaxial iron oxide growth on a stepped Pt(9 11 11) surface

Guido Ketteler*, Wolfgang Ranke

Department of Inorganic Chemistry, Fritz-Haber-Institute of the MPG, Faradayweg 4-6, 14195 Berlin, Germany
*Corresponding author, present address: Lawrence Berkeley National Laboratories, Materials Sciences Division, Mail Stop 66-214, 1 Cyclotron Road, University of California, Berkeley, CA 94720, USA,
e-mail GKetteler@lbl.gov.

Abstract:
In an attempt to introduce steps in oxide surfaces in a controlled way, different iron oxide phases were grown on an atomically stepped Pt(9 11 11) surface. For low coverages, wetting FeO(111) films are formed which induce step bunching with doubled and tripled terrace widths. Further Fe deposition and oxidation results in formation of Fe_3O_4(111) islands in a similar Stranski-Krastanov growth mode as on the basal Pt(111) surface. However, restricted diffusion across the step bunches results in a high concentration of comparatively flat elongated Fe_3O_4 islands which form a closed coalesced film at relatively low overall deposition. High pressure oxidation of coalesced Fe_3O_4 films results in poorly defined Fe_2O_3(0001). The FeO films grown on vicinal Pt substrates may serve as model systems for systematic studies of well-defined defective oxide surfaces, but the catalytically more relevant Fe_3O_4 and Fe_2O_3 phases can not be obtained reproducibly with a well-defined step structure.

1. Introduction

Metal oxides are applied in a wide field spanning from electronic and magnetic devices to heterogeneous catalysis. In this context, structuring of oxide surfaces is increasingly studied[1,2]. The controlled introduction of defects into oxide surfaces may be useful for the identification of reactive surface sites in heterogeneous catalysis. A mechanism that involves defects has been suggested for the catalytic dehydrogenation of ethylbenzene to styrene on iron oxides[3,4].
Due to their lower coordination or modified bond structure, step and kink atoms may be more reactive in gas adsorption and catalysis as also was found in first experiments on metals[5]. In most cases, however, the reactivity of vicinal metal surfaces is surprisingly similar to that of the basal surface plane [6,7] since relaxation and charge redistribution lead to a smeared electron density at step edges. In covalent compounds, the electron density is strongly localized at or between atoms and charge smoothing is not important [8].
Very few studies deal with steps on partially ionic compounds like oxides. Stepped vicinal α-Al_2O_3(0001) surfaces can be created by annealing at 1500°C for several hours[9-11]. Also studies of epitaxial oxide growth on substrates with high step densities are scarce. Hoping to obtain single domain films, some studies were performed for superconducting perovskite oxides on stepped $SrTiO_3$ or MgO substrates[12-14]. More recent studies deal with the growth of epitaxial MgO films on Ag(1 1 19) [15] and the growth of zinc oxide nanowires on vicinal Si(100) [16]. The growth of NaCl, which is isostructural with FeO, has been systematically investigated on Cu(211) [17].
Thin iron oxide films grown epitaxially on Pt substrates were used as model catalysts for the dehydrogenation of ethylbenzene to styrene [18,19]. The growth mode, surface crystallography and defect structure of such films have been characterized on Pt(111) and Pt(100) substrates[20]. Both Fe_3O_4 and Fe_2O_3 are catalytically active with the latter being most active. It has been proposed that defects on Fe_2O_3 play an essential role[3,4]. In an attempt to prepare well-defined defects, we investigate here if atomic steps can be prepared in a controlled way by growing iron oxide films on a stepped Pt(9 11 11) substrate.

2. Experimental

Experiments were performed in an ultra-high vacuum (UHV) chamber with a base pressure of $1x10^{-10}$ mbar. It contains a scanning tunnelling microscope (STM, Burleigh), a combined low-energy electron diffraction (LEED) and Auger electron spectroscopy (AES) optics, and preparation facilities (sputter gun, evaporation source, Ar and oxygen gas inlet valves). For high-resolution spot profile analysis LEED measurements (SPA-LEED), the combined LEED and AES optics was replaced by a SPA-LEED system (Leybold). STM measurements were performed in the constant current mode (~ 1 nA, positive bias <1.3V) with electrochemically etched tungsten tips.

In order to obtain a Pt(9 11 11) surface, a Pt(111) single crystal was cut and polished at an angle of 5.2° towards the $[\bar{2}11]$ azimuth (fig. 1a, b). The nominal average terrace length is 2.48 nm for steps of monoatomic height. For comparison, a facet of the substrate was retained as a basal Pt(111) surface so that the growth on the vicinal surface could be compared directly with the well-known behavior on the basal plane[20]. The miscut angle was chosen so that a coincidence of terrace widths would result for FeO(4 5 5), FeO(15 17 19) and Fe_3O_4(9 9 11). This was hoped to lead to an advantageous heteroepitaxial long-range correlation [21]. For α-Fe_2O_3(0001), no favourable epitaxial relationship was possible.

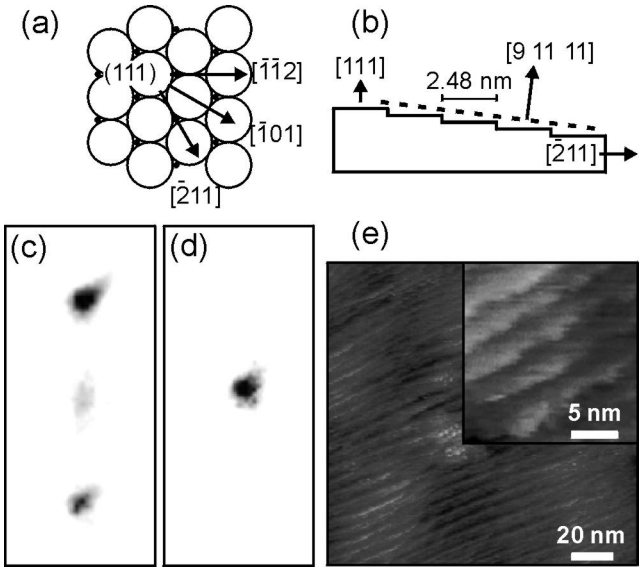

Figure 1:
(a) Top view of Pt(111) with different azimuthal directions. Dots mark 2nd layer atoms. (b) Schematic side view of the Pt(9 11 11) surface. (c) High-resolution SPA-LEED image of the (00) spot at a calculated out-of-phase condition (46eV, S=2.5) and (d) at a calculated in-phase condition (66eV, S=3). (e) STM image of the clean Pt(9 11 11) substrate.

The Pt substrate was cleaned by repeated cycles of Ar sputtering (1 keV, 4-5 μA) and annealing at 1300 K until it exhibited sharp LEED spots and no contamination was detected by AES. Iron was deposited at room temperature by thermal evaporation from an iron wire wrapped around a resistively heated tungsten wire, followed by oxidation. On Pt(111) and Pt(100), the growth follows a modified Stranski-Krastanov mode [22,23]. Initially a thin FeO(111) (wustite) layer (max. 2.5 Fe-O bilayers thick) grows. Then Fe_3O_4 (magnetite) islands form on and into the FeO film. Finally, the islands coalesce into a closed film. This Fe_3O_4 film can be converted into α-Fe_2O_4(0001) (hematite) by oxidation at higher pressures (10^{-4} to 1 mbar) [24,25]. This general growth behavior turned out to be the same on Pt(9 11 11).
Film thickness is given in monolayer equivalents (MLE) as determined by calibration of the Fe source in previous experiments on a Ru(0001) substrate[26]. We estimate the relative error of this calibration to be about 20%. One MLE corresponds to one full Fe-O bilayer of the completely wetting FeO films. In the initially non-wetting Fe_3O_4(111) films, the coverage in MLE corresponds to the average film thickness. As will be shown, the step structure and film morphology depend on the deposition rate. Therefore, amounts between 0.2 and 0.5 MLE of iron were deposited at low (0.06 ML/min) or high rate (3.75 ML/min) either in one turn or cumulative with oxidation after the iron deposition cycles. Oxidation was performed each time either at 870 or at 1000 K in 10^{-6} mbar O_2 for 5-10 min. We were not able to obtain atomic resolution on the stepped surface. Also, the Moire pattern of the FeO films [20] was only visible in the LEED images and not in our STM experiments. As the increase in area covered by more extended terraces is correlated strictly with the calibrated amount of deposited Fe, but not with the oxygen exposure, we can attribute these to FeO. As a double check, we oxidized the vicinal Pt crystal without Fe under the same conditions, and observed no double or triple step formation for the conditions used in our experiments.

3. Results

3.1 Characterization of the clean Pt(9 11 11)

STM investigations of the clean Pt(9 11 11) substrate confirm the expected average terrace width of about 2.5 nm and the existence of monoatomic steps (fig. 1e). The step edges are not always straight, and occasionally an increased number of kink atoms occur. LEED shows the typical diffraction pattern of the (111) surface terraces with step-induced spot splitting. High-resolution SPA-LEED measurements of the specular beam at a calculated out-of-phase scattering condition (46eV, S=2.5) show a maximum splitting corresponding to an average terrace length of 2.46 nm (fig. 1c) which agrees perfectly with the nominal average terrace length of 2.48 nm. However, the existence of a residual weak central peak indicates some variance in the terrace width distribution in agreement with the kinks observed in STM. As expected, only a single spot is visible at a calculated in-phase scattering condition (fig. 1d).

3.2 Growth of iron oxides at low deposition rate

Already for low Fe depositions, followed by oxidation at 870 K, morphology changes occur. The narrow terraces in fig. 2a, b represent uncovered Pt regions with single layer steps. The expanded terraces are covered by a single bilayer FeO film. Here,

most step heights are tripled, some are doubled. With increasing coverage, terrace widths vary more strongly but are always larger than on the uncovered Pt substrate (fig. 2c, d). The FeO islands are never wider than the expanded terraces. Obviously Fe and possibly also O can diffuse across steps until they are bound to FeO islands which then grow only along the terraces. Further increase of the coverage leads already to nucleation of Fe_3O_4(111) islands (fig. 2f). Different than growth on Pt(111), this appears to occur before the full FeO layer is established. We ascribe this to local concentration variations of iron and hindered diffusion across steps. The Fe_3O_4 islands are oriented and elongated along the step edges. Between them, the stepped FeO structure is quite irregular with many kink sites (fig. 2e). The average edge orientation is still the same as on the original Pt substrate. Further Fe deposition and oxidation (fig. 3a-c) leads to an increased number and size of the Fe_3O_4(111) islands. Although less prominent, also the coalesced film (fig. 3c) still shows the edge-induced texture. Before coalescence, (fig. 3a, b), the FeO step structure between the islands becomes more regular.

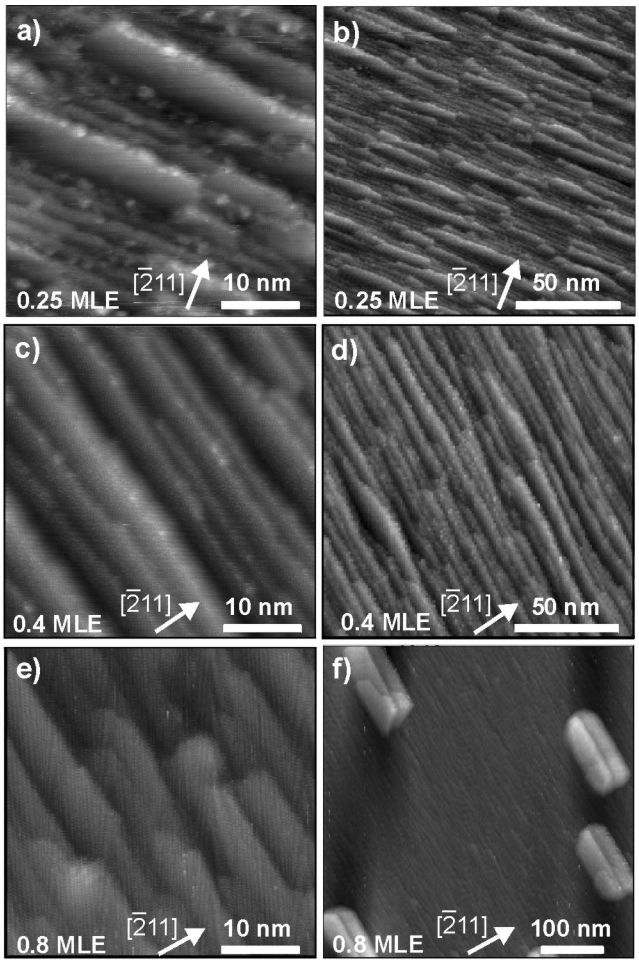

Figure 2:
STM images of consecutive growth stages of FeO at low Fe flux. Oxidation in 10^{-6} mbar O_2. (a-d) One-turn Fe deposition, oxidation at 870 K; (e, f) Cumulative Fe deposition, oxidation at 870 K. Although the FeO layer in (f) is not yet closed, Fe_3O_4 islands have formed, see text. The double-edge structure in these islands is a tip artefact.

The STM observations are confirmed by SPA-LEED measurements (fig. 4). Although the Pt substrate in fig. 4 a, b is only partially covered by FeO, the LEED pattern is completely dominated by the oxide film because its spot intensities are much higher. As for thin FeO(111) films on Pt(111), multiple-scattering satellites appear around the FeO-derived spots[20]. Due to the step structure of the films, the main diffraction spot and also the satellite reflections are smeared to streaks perpendicular to the edge direction. For low coverages, the streaked main diffraction spot has two maxima (fig. 4a). Their distance corresponds to a doubled average terrace width. At slightly higher coverage, occasionally also a splitting corresponding to triple step heights could be resolved (fig. 4b). With increasing coverage, the splitting vanishes and finally, the spot assumes a sharper oval shape (fig. 4d). At this stage, the surface is mainly covered by Fe_3O_4 islands with low defect density as in fig. 3c. The oval spot shape reflects the elongation of these islands. However, the weak residual satellite spots in fig. 4d are the signature of FeO(111) and show that the Fe_3O_4 film is not yet completely closed.
Corresponding growth studies were performed applying higher oxidation temperatures (1000 K). Generally, the same Stranski-Krastanov growth of Fe_3O_4 islands on a closed FeO(111) layer is observed without improvement of ordering or regularity of step spacings. However, the shape of the nucleating Fe_3O_4(111) islands is different. At 870 K, they are elongated along step edges (fig. 3c), while at 1000 K a preferentially trigonal or hexagonal morphology forms (fig. 3d) which is similar to that observed on the basal Pt(111) [22]. Only in the orientation of these island an alignment effect along the nominal edge direction is still visible. The high temperature is thus beneficial for the formation of the equilibrium crystal shape. LEED shows the well-known Fe_3O_4(111) pattern with sharp, round spots. The islands are terminated by extended (111) planes without increased concentrations of defects or steps compared to Fe_3O_4(111) islands grown on unstepped substrates.

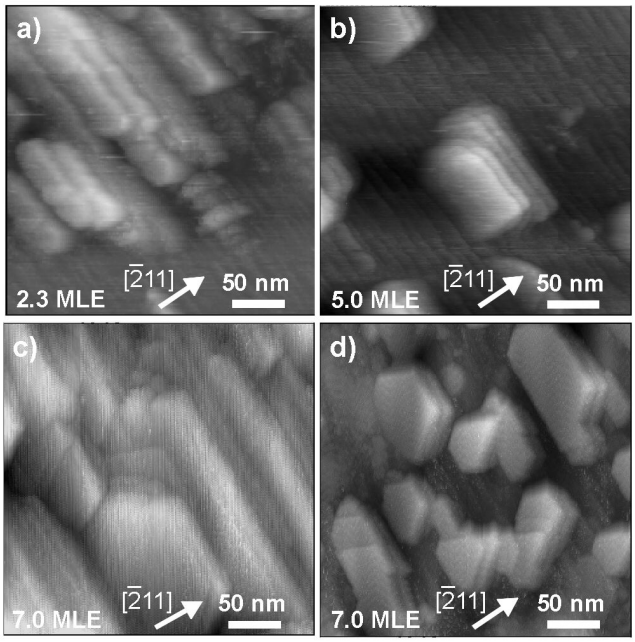

Figure 3:
STM images for consecutive growth stages of Fe_3O_4 islands with cumulative deposition at low Fe flux. (a-c): Oxidation at 870 K in 10^{-6} mbar O_2. (d): Oxidation at 1000 K in 10^{-6} mbar O_2. The edge structure of Fe_3O_4 islands in (b,d) is disturbed by double-tip effects of the STM tip.

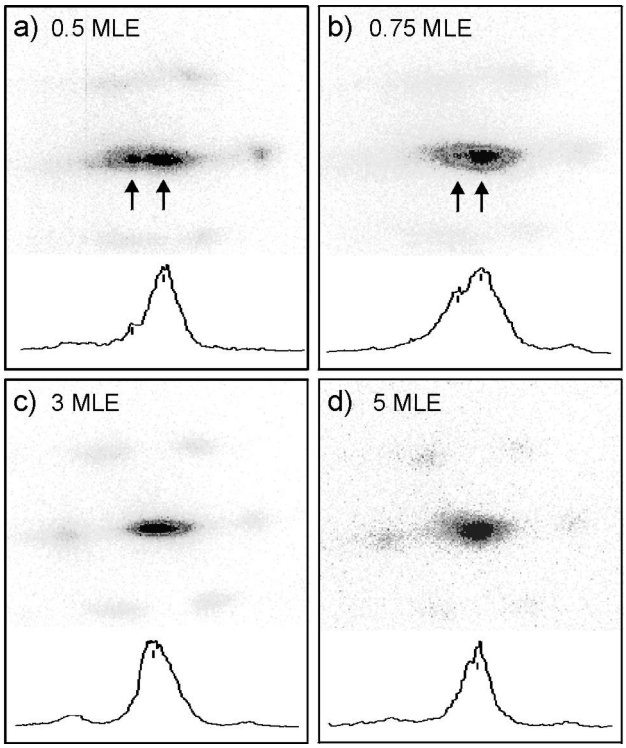

Figure 4:
SPALEED images (E_p=90eV) and two-dimensional cross-sections along the streak directions of the (00) diffraction beam of iron oxide films deposited at low flux and oxidized at 870K. The box lengths correspond to about 40% of the (00)-(01) distance of the Pt(111) pattern. (a) One-turn deposition, 0.5 MLE, FeO pattern; (b) 0.75 MLE cumulative deposition, FeO pattern; (c) 3 MLE cumulative deposition, Fe_3O_4+FeO pattern; (d) 5 MLE cumulative deposition, Fe_3O_4+weak FeO pattern.

Fe_3O_4(111) films grown on Pt(9 11 11) were oxidized completely to α-Fe_2O_3(0001) by heating them in 10^{-1} mbar O_2 for 15 min. at 1100K. The LEED pattern and large scale STM images of an Fe_3O_4(111) film before and after oxidation are shown in fig. 5. After oxidation, the LEED pattern has completely changed to that of Fe_2O_3 (fig. 5c) but the background has increased. STM confirms a reduced long-range order (compare fig. 5d with 5b). The Fe_2O_3 domains have no preferential orientation. Thus, although the defect density of Fe_2O_3(0001) on a vicinal Pt substrate is significantly increased, no systematic introduction of well-defined defect structures seems possible.

3.3 Growth of iron oxide at high deposition rate

Results for growth by one turn deposition at high rate (~3.75 ML/min) followed by oxidation at 870 K are shown in fig. 6. After deposition and oxidation of ~0.2 MLE, the average terrace width of Pt(9 11 11) is unchanged but the number of kink sites has increased significantly and the edges are rougher (fig. 6a). On some parts, deposits with a cluster morphology are resolved (upper part of fig. 6b). No extended FeO covered terraces are formed and no oxide-related LEED spots are visible indicating that the iron oxide film is not well ordered at this stage. Although FeO covered domains in fig. 6a can hardly be distinguished from bare Pt, the generally increased edge roughness shows that Pt substrate atoms were displaced.

Larger deposited and oxidized amounts (0.6 MLE, fig. 6c,d) change the step structure dramatically. The average terrace width has significantly increased, showing step height doubling and tripling, similar to the case of low deposition rate. The edges are, however, rougher. Sometimes, tripled terraces are quite regularly spaced (fig. 6c). At this stage, LEED patterns from FeO(111) similar to fig. 4 are observed.
It was not possible to improve the step regularity by longer oxidation. Even deposition of a full monolayer and oxidation at higher temperatures did not result in ordered, regularly spaced step patterns. Fig. 6e, f shows that oxidation at 1000 K instead causes increased roughness on the step bunches.

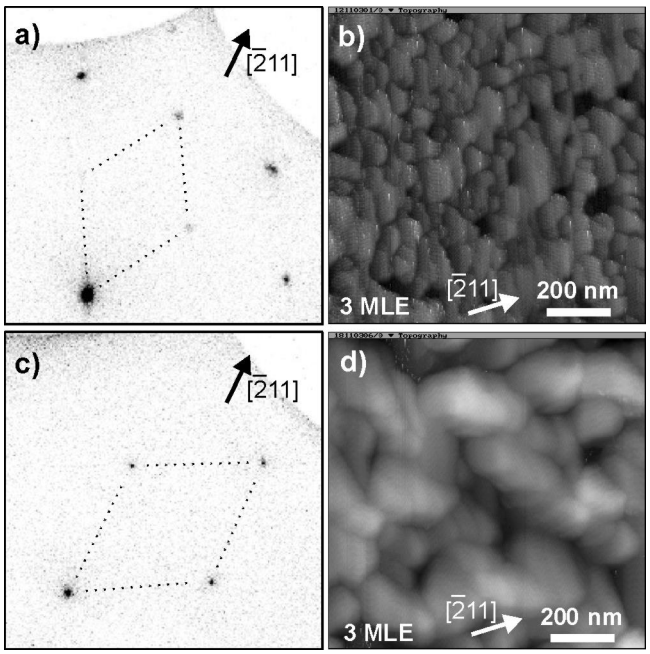

Figure 5:
(a) 70eV LEED image and (b) STM image of a coalesced Fe_3O_4(111) film, slow cumulative deposition. (c) 90eV LEED image and (d) STM image of the same film after high pressure oxidation to α-Fe_2O_3(0001). The LEED images are taken with the SPA-LEED optics. The lower left intense spot is the (0,0) spot, the surface unit cells are indicated.

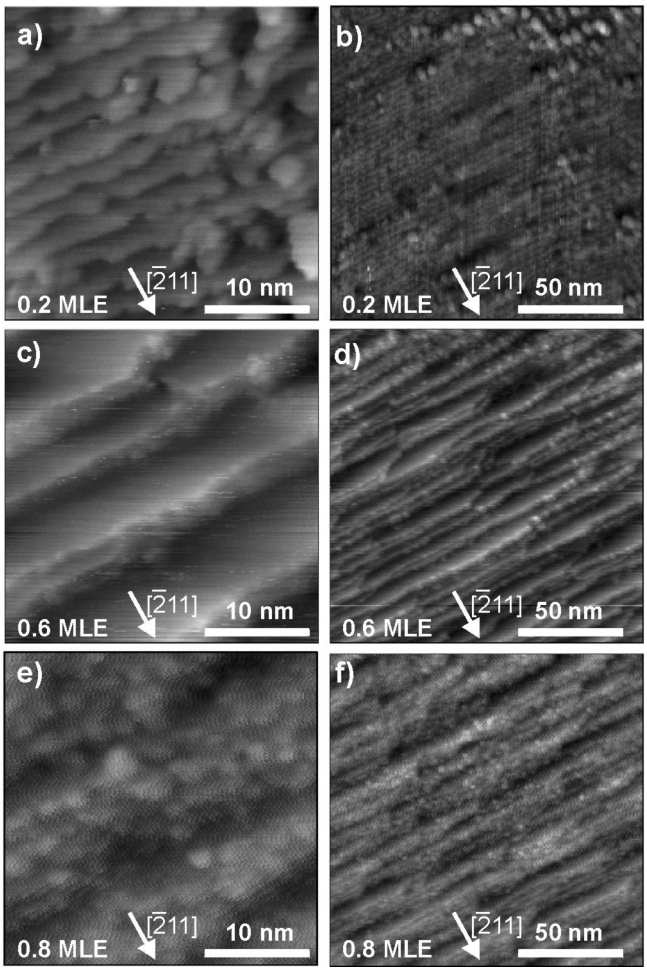

Figure 6:
Growth of FeO, one-turn deposition with high Fe flux and oxidation in 10^{-6} mbar O_2. (a-d): Oxidation at 870 K; (e, f): Oxidation at 1000 K.

4. Discussion

In epitaxial growth, the energy balance $\Delta\gamma = \gamma_f + \gamma_{in} - \gamma_s$ governs the growth morphology [27] (γ_f , γ_s: surface free energy of the deposited film and a substrate, respectively; γ_{in}: interface free energy): For $\Delta\gamma > 0$, compact islands or clusters are formed (Volmer-Weber growth mode) while for $\Delta\gamma < 0$ wetting layers with a high surface and interface area are expected (Frank-Van der Merwe growth mode). The surface free energy of oxides is usually lower than that of metals, therefore wetting of the metal substrate is expected as long as the interface free energy is neglible, a condition which may often not be fulfilled due to lattice mismatch induced strain or specific interactions at the interface. For epitaxial iron oxide growth on Pt(111), Pt(100) and Ru(0001) basal planes, [22,26,28] a modified Stranski-Krastanov (island-on-film) growth was found: Initially, a wetting FeO(111) coincidence layer forms up to a thickness of 1 to 4 ML, then Fe_3O_4(111) islands form on and into the FeO layer, grow and eventually coalesce into a closed film. The present study shows that this principal growth behaviour also applies to stepped Pt substrates.

Surface irregularities and defects may significantly influence the growth mode and energetics[29]. Steps and kinks lead to a higher contact area and the interface energy gains importance. Further, preferential nucleation at such defect sites can be expected when the condition $\Delta\gamma>0$ or $\gamma_{in} < \gamma_s + \gamma_f$ is fulfilled at the steps[27]. Thus, it was observed for FeO growth on Pt(111), that growth occurs preferentially on the lower terrace along edges of widely separated steps[22]. This interaction even induces edge roughening and deficiency island formation on the Pt substrate when oxidation is performed at sufficiently high temperature (at 1000 K but not yet at 870 K). Increased disorder was the result; step bunching did not occur. The present study shows that restructuring by step bunching already occurs at lower temperature (870 K) on a surface with high step density.

Previous studies have shown that also adsorption of gases may lead to morphology changes of vicinal surfaces[5,30]. For instance, the average terrace width of Pt(9 9 7) and Pt(10 10 9) is doubled in an oxygen atmosphere[31-33]. The adsorption of oxygen changes the surface free energy of the terraces and/or step and kink energies in a way which favours terrace width doubling. However, the oxygen atmosphere during Fe oxidation on the Pt(9 11 11) surface studied here does not change the the terrace morphology in regions not covered by FeO (see fig. 2a), probably because oxygen does not adsorb on Pt at the elevated temperature.

The driving force for the adlayer induced morphological changes must therefore be the low surface free energy of ultrathin FeO(111) films. On metals, the surface free energy of vicinal surface planes is similar to that of the basal plane ($\gamma_{s,vicinal}(Me) \geq \gamma_{s,basal}(Me)$) because the electron density in metals is easily smeared at edges. Thus, the energy difference between the vicinal surface and the lower-energy combination of low-index facets for Ag amounts only to ~1% [34]. For Pt, the difference between the various vicinal faces and the (111) plane is less than 0.02 eV per step atom[35]. Due to the more localized character of the partially covalent bonds in oxides, this difference may be much higher ($\gamma_{s,vicinal}(Ox) >> \gamma_{s,basal}(Ox)$)[36]. Extended basal terraces as found in our case will be formed if the nanofacets formed by step bunching are energetically favorable compared to the corresponding concentration of single layer steps. Due to the low difference in surface free energy, the metal substrate probably can easily adjust to the new morphology.

For the mechanism of restructuring, the tendency of Fe to alloy with Pt may be important. Even at 300K, Fe may penetrate into the first Pt layer(s) and induce disorder and displacement of Pt atoms. If oxidation is activated, alloying and Pt displacement may initially be accelerated during heating in oxygen until finally oxidation takes over and accumulates the iron in the oxide. The rearrangement of the substrate would then occur in the most favorable configuration with extended terraces.

The resulting terrace widths are expected to be kinetically limited. The preferential formation of doubled and tripled terrace widths, however, suggest a favourable double or triple step structure. In our case, the FeO islands are only 1 bilayer (bulk value 0.25 nm) high, which is considerably less than two (0.45 nm) or three (0.68 nm) Pt layers, and they do not overgrow the steps (fig. 2a). FeO steps are thus not formed and the favourable double or triple edge structure must consist of the combination of a high Pt step with an FeO layer attached to it on the higher and/or lower terrace.

The lowest coverages in fig. 2a, b and fig. 6a, b differ in the deposition rate, which was almost 20 times faster in fig.6, while the oxidation treatment was identical. That slow Fe deposition resulted in the formation of well shaped FeO islands on expanded terraces may be explained by the tendency of Fe to form clusters on Pt surfaces[20]. Clustering requires diffusion, and the longer interaction time during slow deposition rates thus is expected to result in less but larger Fe clusters. As these are the nucleation sites for FeO during oxidation, these differences may be the reason for the differences in morphology.

That the surface order for higher coverages at slow deposition is better is easy to understand. These coverages were the result of cumulative exposure with oxidation at 870 K in between.

The growth of Fe_3O_4 islands is strongly influenced by the underlying step structure. On the basal Pt(111) surface[22], the islands are triangular or hexagonal. Their diameter is 200 to 500 nm and their height 2-5 nm. Closed films thinner than about 100 nm can hardly be obtained. On the stepped Pt(9 11 11) surface, the same preparation conditions (oxidation at 870 K) result in elongated islands with their parallel long edges aligned along the substrate step direction (fig. 2f, fig. 3a-c). Isolated islands are about 50 nm wide and 100 nm long (fig. 2f). The height of the islands is considerably smaller than on basal Pt(111) and their concentration higher. Therefore, they coalesce into a closed film upon deposition of only 3 to 10 MLE (fig. 5b) which corresponds to 1-2 nm. The width of the islands has then not increased much, their length is 100-200 nm. Instead of growing in height as on the basal Pt(111) surface, the nucleation sites offered by the substrate steps and the restricted diffusion across steps causes growth of a high concentration of flat islands. This structure is kinetically stabilized. When the oxidation temperature is raised to 1000 K (fig. 3d) the island shape changes. In addition to islands elongated along the edge direction, also triangular and hexagonal islands as on basal Pt(111) appear.

On the Pt(9 11 11) surface it is thus possible to prepare much thinner Fe_3O_4 films than on Pt(111). The domains are generally smaller and, when oxidized at 870 K, elongated along the edge direction. The defect concentration is high but a well-defined stepped surface cannot be prepared.

5. Conclusions

The introduction of step defects in oxide surfaces is difficult due to the generally high surface free energy of vicinal oxide planes compared to the basal plane. Deposition of a thin FeO layer on a stepped Pt(9 11 11) surface causes step bunching with double and triple terrace widths. As on the basal Pt(111) surface, further growth proceeds in a modified Stranski-Krastanov mode with Fe_3O_4(111) islands forming on the initial wetting FeO(111) layer. Eventually, the Fe_3O_4 islands coalesce into a closed film with step-induced texture. High pressure oxidation to Fe_2O_3, the iron oxide phase with the highest catalytic activity for the dehydrogenation of ethylbenzene to styrene, results in ill-defined defect structures with poor long-range order. Only the thin initial FeO(111) films are promising candidates for systematic studies of step defects.

Acknowledgements

We thank Robert Schlögl for fruitful discussions and continuous support of this project.

References

1. H. Brune, M. Giovannini, K. Bromann, and K. Kern, Nature **394**, 451 (1998).
2. P. Gambardella, A. Dallmeyer, K. Maiti, M. C. Malagoli, W. Eberhardt, K. Kern, and C. Carbone, Nature **416**, 301 (2002).
3. W. Weiss, D. Zscherpel, and R. Schlögl, Cat. Lett. **52**, 215 (1998).
4. Y. Joseph, M. Wühn, A. Niklewski, W. Ranke, W. Weiss, C. Wöll, and R. Schlögl, Phys. Chem. Chem. Phys. **2**, 5314 (2000).
5. B. Lang, R. W. Joyner, and G. Somorjai, Surf. Sci. **30**, 440 (1972).
6. W. T. Lee, L. Ford, P. Blowers, H. L. Nigg, and R. I. Masel, Surf. Sci. **416**, 141 (1998).
7. L. P. Ford, P. Blowers, and R. I. Masel, J. Vac Sci. & Tech. A **17**, 1705 (1999).
8. H. J. Kuhr and W. Ranke, Solid State Comm. **61**, 285 (1987).
9. M. Lintz and M. A. Bouchiat, Surf. Sci. **511**, L319-L324 (2002).
10. J. R. Heffelfinger, M. W. Bench, and C. B. Carter, Surf. Sci. **343**, L1161-L1166 (1995).
11. L. Pham Van, J. Cousty, and C. Lubin, Surf. Sci. **549**, 157 (2004).
12. V. C. Matijasevic, B. Ilge, B. Stäuble-Pümpin, G. Rietveld, F. Tuinstra, and J. E. Mooij, Phys. Rev. Lett. **76**, 4765 (1996).
13. C. D. Theis, J. Yeh, D. G. Schlom, M. E. Hawley, and G. W. Brown, Mat. Sci. Eng. **B56**, 228 (1998).
14. R. A. Rao, Q. Gan, and C. B. Eom, Appl. Phys. Lett. **71**, 1171 (1997).
15. J. Kramer, C. Tegenkamp, W. Ernst, and H. Pfnür, Surf. Sci. **537**, 265 (2003).
16. J. S. Lee, M. I. Kang, S. Kim, M. S. Lee, and Y. K. Lee, J. Cryst. Growth **249**, 201 (2003).
17. S. Fölsch, A. Helms, A. Riemann, J. Repp, G. Meyer, and K. H. Rieder, Surf. Sci. **497**, 113 (2002).
18. O. Shekhah, W. Ranke, A. Schüle, G. Kolios, and R. Schlögl, Angew. Chem. Int. Ed. **42**, 5760 (2003).
19. O. Shekhah, W. Ranke, and R. Schlögl, J. Cat. **225**, 56 (2004).
20. W. Weiss and W. Ranke, Prog. Surf. Sci. **70**, 1 (2002).
21. Y. Garreau, A. Coati, A. Zobelli, and J. Creuze, Phys. Rev. Lett. **91**, 116101 (2003).
22. W. Weiss and M. Ritter, Phys. Rev. B **59**, 5201 (1999).
23. M. Ritter, H. Over, and W. Weiss, Surf. Sci. **371**, 245 (1997).
24. S. K. Shaikhutdinov and W. Weiss, Surf. Sci. **432**, L627 (1999).
25. G. Ketteler, W. Weiss, and W. Ranke, Surf. Rev. Lett. **8**, 661 (2001).
26. G. Ketteler and W. Ranke, J. Phys. Chem. B **107**, 4320 (2003).
27. E. Bauer, Z. Kristall. **110**, 372 (1958).
28. S. Shaikhutdinov, M. Ritter, and W. Weiss, Phys. Rev. B **62**, 7535 (2000) 7535.
29. G. Ketteler and W. Ranke, Mat. Res. Soc. Symp. Proc. **775**, P6.1.1 (2003).
30. D. W. Blakely and G. Somorjai, Surf. Sci. **65**, 419 (1977).
31. E. Hahn, H. Schief, V. Marsico, A. Fricke, and K. Kern, Phys. Rev. Lett. **72**, 3378 (1994).
32. G. Comsa, G. Mechtersheimer, and B. Poelsema, Surf. Sci. **119**, 159 (1982).
33. E. Herrero, J. M. Orts, A. Aldaz, and J. M. Feliu, Surf. Sci. **440**, 259 (1999).
34. J. W. M. Frenken and P. Stoltze, Phys. Rev. Lett. **82**, 3500 (1999).
35. P. J. Feibelman, Phys. Rev. B **52**, 16845 (1995) 16845.
36. P. W. Tasker and D. M. Duffy, Surf. Sci. **137**, 91 (1984).